THE JOURNAL OF PHYSICAL CHEMISTRY C

Article

pubs.acs.org/JPCC

A Practical Criterion for Screening Stable Boron Nanostructures

Shao-Gang Xu,[†,‡] Yu-Jun Zhao,[†] Xiao-Bao Yang,[*,†,‡] and Hu Xu[*,‡]

[†]Department of Physics, South China University of Technology, Guangzhou 510640, P. R. China

[‡]Department of Physics, South University of Science and Technology of China, Shenzhen 518055, P. R. China

Supporting Information

ABSTRACT: Due to the electron deficiency, boron clusters evolve strikingly with the increasing size as confirmed by experimentalists and theorists. However, it is still a challenge to propose a model potential to describe the stabilities of boron. On the basis of the 2c-2e and 3c-2e bond models, we have found the constraints for stable boron clusters, which can be used for determining the vacancy concentration and screening the candidates. Among numerous tubular structures and quasi-planar structures, we have verified that the stable clusters with lower formation energies bounded by the constraints, indicating the competition of tubular and planar structures. Notably, we have found a tubular cluster of B_{76} which is more stable than the B_{80} cage. We show that the vacancies, as well as the edge, are necessary for the 2c-2e bonds, which will stabilize the boron nanostructures. Therefore, the quasi-planar and tubular boron nanostructures could be as stable as the cages, which have no edge atoms. Our finding has shed light on understanding the complicated electron distributions of boron clusters and enhancing the efficiency of searching stable B nanostructures.

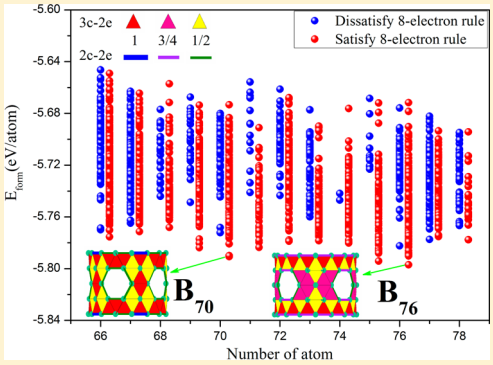

1. INTRODUCTION

Boron structures have been attractive due to the large variety with the increasing sizes, attributed to the electron deficiency.[1−4] The isolated B_{12} cluster is a planar triangular fragment, while 12 B atoms form a highly symmetric icosahedra in the α-rhombohedral bulk.[5] Confirmed by the experiment observation and *ab initio* calculations, there are several typical structures which can coexist as low-lying isomers: (1) quasi-planar, B_{21}^-, B_{23}^-, B_{24}^-, B_{25}^-, B_{27}^-, B_{30}^-, B_{35}^-, and B_{36};[6−13] (2) tubular, B_{18}^+, B_{20}, B_{22}^+, B_{24}^+, and B_{27};[14−16] (3) cage-like, B_{28}, B_{29}, B_{38}, B_{39}^-, and B_{40}.[17−22] Planar B nanostructures with a convex profile are stable in vacuum, whereas they would be not stable when deposited on metal surfaces, which would evolve with the size[23,24] and form boron sheets with various patterns of vacancies,[25,26] verified by recent experiments.[27,28]

As is known, the variety of carbon hollow cages and planar graphene nanoflakes is attributed to the stable sp^2 hybridizations of carbon, since these nanostructures have the same motifs with the graphene sheet.[29] Similarly, the B_{80}[30] cluster can be considered as the corresponding cage of the α sheet,[31,32] while the B_{56} and B_{84} clusters are the fragments of the α sheet.[33] However, the detailed configurations are found to be strongly dependent on the number of boron atoms, according to the larger quasi-planar structures of B_n found in our previous study.[34] As the number of boron atoms increases, the tubular structures with hexagonal vacancies might become stable, though there are still a few problems to be answered, such as the thickness of tubular structures, as well as the concentration and distribution of the vacancies in the tubes. In addition, it is lacking a rule to help us screen the stable boron nanostructures from the enormous possible candidates.

In this paper, we have combined high-throughput[35] screening with the first-principles calculation to search possible tubular and quasi-planar boron nanostructures. According to our bond model,[34] we determine the proper interval of vacancy concentration for a given candidate. The vacancies are generally distributed with high symmetry to stabilize the system, while there are some exceptional examples. It is found that there will be a solution for any stable structure following the bond model with the 8-electron rule, which can be used to screen the candidates efficiently. From over 5000 candidates, we have found the effective geometrical constraints to determine the vacancy concentration and screen the candidates, since both the distribution and the concentration of the vacancies are crucial to the stability of the B_n clusters. We also found a few highly stable B_n clusters (B_{70}, B_{76}), where the B_{76} is energetically more stable than the predicted B_{80} fullerene.[30] The effective model we proposed recently[34] can successfully help us understand the stability of the B_n cluster, based on only two-center two-electron (2c-2e) and three-center two-electron (3c-2e) bonds distribution.

2. COMPUTATIONAL METHODS

The first-principles calculations of B_n candidates were based on the density functional theory (DFT) implemented in the Vienna *Ab initio* Simulation Package (VASP)[36,37] method. The projector augmented wave (PAW) method and the Perdew−

Received: April 9, 2017
Revised: May 14, 2017
Published: May 16, 2017

DOI: 10.1021/acs.jpcc.7b03359
J. Phys. Chem. C 2017, 121, 11950−11955

Burke−Ernzerhof (PBE) of the generalized gradient approximation (GGA) functional[38,39] were employed for the total energies calculations. The energy cutoff was 480 eV, and the criteria of the forces on each atom were set to be 0.02 eV/Å. To avoid the cell-to-cell interactions, the vacuum distance was carefully tested. We also used the DMol[340,41]method combined with the exchange-correlation functional of GGA (PBE) for comparison. In addition, we have performed the calculation with the hybrid functional of Heyd−Scuseria−Ernzerhof (HSE06),[42,43] to confirm the energy gaps between the highest occupied molecular orbital (HOMO) and lowest unoccupied molecular orbital (LUMO) in higher accuracy.

Combined with a congruence check, we obtained all the possible isomers for any given number of atoms, including the candidates of planar and tubular ones. The tubular candidates are constructed by rolling the triangular lattice with various distributions of vacancies, where the details for the congruence check are shown in the Supporting Information (SI). To explain the structural stabilities and charge distribution, we have proposed an effective model[34] based on two main assumptions: (i) s 2c-2e bonds and t 3c-2e bonds are introduced for B_n clusters to satisfy the 8-electron rule for every B atom (i.e., $2s + 2t = 3n$ and $4s + 6t = 8n$); (ii) the distribution of 2c-2e and 3c-2e bonds should be in agreement with the charge difference and the configuration's symmetry. In our model, the occupations of 2c-2e and 3c-2e bonds are from 0 to 1, where the variance of distribution is minimized to describe the delocalized bonding, while the 8-electron rule indicates the localized characteristic.

3. RESULTS AND DISCUSSION

First, we show why the vacancy is necessary and give the proper interval of vacancy concentration. Second, we have considered the symmetry effect and confirmed the 8-electron model constraint for possible stable clusters, determining the stable planar and tubular structure for the size of 50−85 atoms. Finally, we present the distributions of 2c-2e and 3c-2e bonds for the corresponding magic number B_n clusters.

3.1. The Proper Interval of Vacancy Concentration. In our recent work, we have proposed a simple model to analyze the distributions of 2c-2e and 3c-2e bonds in boron clusters, which is in agreement with the charge difference from the first-principles calculations. To satisfy the 8-electron rule, there are $0.5n$ 2c-2e bonds and n 3c-2e bonds for B_n clusters, respectively, where the 2c-2e bonds are found to be located on the peripheral edges with the 3c-2e bonds on the triangles. Thus, a stable B_n cluster should have more than $0.5n$ edge and n triangles for the 2c-2e and 3c-2e bonds, respectively. As shown in Figure 1, we have checked the reported B_n ($n \geq 20$) clusters and confirmed that all of these stable clusters satisfy this constraint. Extending the constraint for the infinite planar B sheet, we can obtain the proper concentration of hexagon vacancy for the possibly stable borophene: for a cell of triangular lattice with n^2 atoms and $2n^2$ triangles, one hexagon vacancy would produce six edge bonds, which would reduce the number of atoms and triangles by one and six, respectively. There are two constraints: (1) $0.5 \times (n^2 - 1) \leq 6$, (2) $(n^2 - 1) \leq (2n^2 - 6)$ to ensure that there are enough edges and triangles for 2c-2e and 3c-2e bonds. Thus, the vacancy concentration η for the reasonable B sheets is $1/13 \leq \eta \leq 1/5$, which agrees with the results reported before.[31] Note that the constraint of vacancy concentration would help us screen the candidates effectively. For a 6×6 triangular lattice supercell, only 0.0156% initial structures among the total 2^{36} possible candidates satisfy the η constraint.

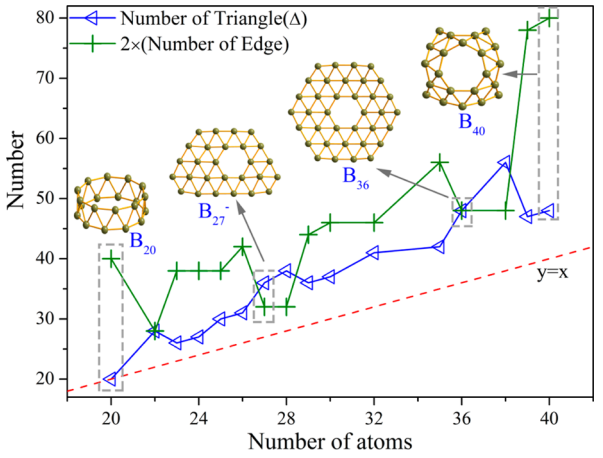

Figure 1. Relation of the number of triangles (edges) and the size of the reported B_n clusters. The blue triangle represents the number of triangles for the corresponding B_n clusters; the green cross represents the number of the edges for the corresponding B_n clusters. The geometry structures of the B_{20}, B_{27}^-, B_{36}, and B_{40} cage confirmed by the experiments are presented in the figure.

For an N-ring structure with m atoms in a single ring, the number of triangles in the tubular clusters is $2 \times (N - 1) \times m$ and the number of edges at both sides is $2 \times m$. According to the two conditions of our 8-electron rule, we can get $2 \leq N \leq 4$. Thus, the structure with $N > 4$ should be unstable and vacancies should be introduced to increase the edges for 2c-2e bonds. To verify this, we calculated a few triangular lattice B nanoribbons of different widths and the corresponding B_n rings with various diameters. As shown in Figure S2, we have calculated the average formation energy (E_{form}) for B_n ($n \leq 100$) clusters with the structures of (2−6) triangular lattice rings. As the size of the cluster increases, the three-ring tubular clusters are more stable than other tubular structures of B_n ($30 \leq n \leq 100$), in agreement with previous studies.[44,45]

Figure 2 shows the structural stabilities of boron nanoribbons with/without vacancies as a function of the width. There is a local minimal at $N = 3$ for the ribbons without vacancies. Introducing one hexagonal vacancy for the N-layer ($N \geq 5$) ribbons, the systems can be dramatically stabilized. The inset of Figure 2 shows the possible boron structures from a five-ring B_{80} tubular cluster, where 2−6 vacancies are required to satisfy the constraint of vacancy constraint. The ground state structures of B_{74-78} are more stable than $B_{79,80}$, where the B_{76} with 4 hexagonal vacancies is the most stable one for the given five-ring structures.

3.2. The Distribution of Vacancies in Stable Boron Nanostructures. As shown in the inset of Figure 2, constraint of vacancy concentration is always not enough. The constraint could be further refined according to the distributions of hexagon vacancies. In our recent work,[34] we have screened all the possible planar B_n (n = 30−51) isomers with 1−2 hexagonal vacancies with the profile $\{n_1n_2n_3\}$, checking the 12 symmetry operations (SOs) of triangular lattice. As shown in Figure 3a, there are four isomers for the B_{36} from the {744} profile with one hexagonal vacancy, where the atoms (a−d) in dark represent the possible positions for the vacancies. For B_{36}, the structure (1) (cf. Figure 3a) with the most SOs is more stable than the others with less SOs by around 1.7−4.1 eV in

DOI: 10.1021/acs.jpcc.7b03359
J. Phys. Chem. C 2017, 121, 11950−11955

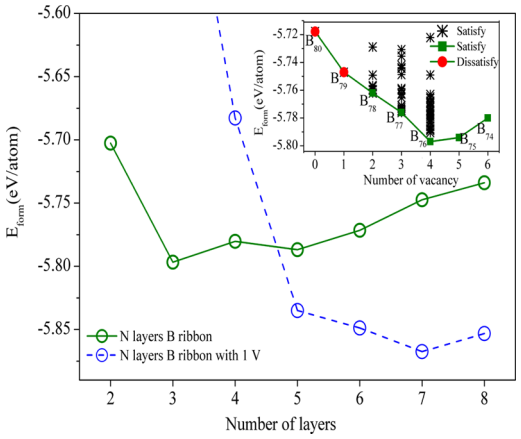

Figure 2. Relation of the average formation energy (E_{form}) and the layers (N) of the B nanoribbon. The green solid line represents the relation of the E_{form} and the B N-layer nanoribbon; the blue dashed line represents the relation of the E_{form} and the B N-layer nanoribbon with one hexagonal vacancy (V) in the middle. All the dots in the inset represent E_{form} of the isomers constructed by the five-ring B_{80} tubular clusters with a few hexagonal vacancies. The red dots represent the structures that dissatisfy our constraint; the other dots represent the structures that satisfy the constraint.

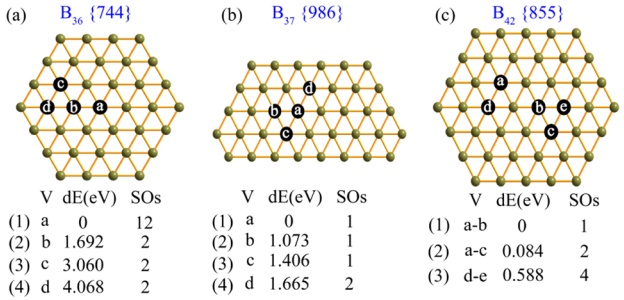

Figure 3. Initial structures of the B_n (n = 36, 37, 42) quasi-planar clusters and their relative total energy in GGA (PBE) level; the number of the symmetry operations (SOs) for the corresponding structures are shown at the downside. Parts (a) and (b) represent the initial structure of B_{36}, B_{37} with the profile of {744} and {986} accompany a hexagonal vacancy (V), marked by a-d. Part (c) represents the initial structure of B_{42} with the profile of {855} accompany a double hexagonal vacancy, marked by (a-b, a-c, d-e), respectively.

total energies. However, for the B_{37} (Figure 3b-1) and B_{42} (Figure 3c-1), the structures with less SOs are more stable than those with more SOs. For example, the total energy of the B_{42} isomer with a double-vacancy (*d-e*, number of SOs = 4) is 0.588 eV higher than the one with a double-vacancy (*a-b*, number of SOs = 1).

Figure 4a shows the symmetry of boron planar clusters with the number from 32 to 50, where most of the stable structures are of high symmetry with SOs ≥ 1, especially for the magic number clusters. Meanwhile, there are several stable clusters with SOs = 1 (B_{37}, B_{42}, B_{48}). As the size of the clusters increases, the number of isomers for the planar clusters is out of our computational capabilities. To further reduce the number of candidates, we have adopted a 2c-2e and 3c-2e bond model to analyze the boron clusters, determining the bond distributions to ensure every B atom satisfies the 8-electron rule.[34] We have checked whether there is a solution for all the calculated structures based on the bond model with the 8-electron rule. As shown in Figure 4b, the initial planar structures with model solutions are always more stable than that without solutions, indicating that we can screen the candidates by checking them first to find if there is a solution. Combined with the 8-electron rule screening, about 64% of initial structures can be further eliminated, which reveals the efficiency of the model analysis.

We have searched the possible stable B_n clusters with larger sizes by the congruence check, including the tubular ones and quasi-planar ones (shown in Figure S3). The ground state structures of boron clusters will vary as a function of the number of boron atoms, where the three-ring tubular clusters are more stable at $40 < n \leq 63$, while the five-ring tubular ones with hexagonal vacancies become more and more stable with $n > 63$. For the quasi-planar B_n clusters shown in Figure S3d, more hexagonal vacancies should be introduced to stabilize the systems of larger sizes. In addition, the model constraint based on the 8-electron rule can help us screen the initial structures effectively for both quasi-planar and tubular clusters, as shown in Figure S4. The structures of all the stable B_n clusters are presented in the SI (Figure S5).

3.3. The 2D−3D Evolution of Boron Nanostructures.

In the following, we focus on the local minimum of the tubular clusters and the quasi-planar clusters in Figure 5. For the boron clusters of smaller size, B_{36} is a magic quasi-planar cluster with C_{6v} symmetry,[12] and the tubular B_{42} is another magic number cluster. The B_{42} cage[46] is even less stable than the quasi-planar B_{36}. As the size increases, the local minimum of the quasi-planar clusters (the dashed line with square dots) B_n (n = 36, 56, 70, 84) have been considered to be the fragments of the α B sheet.[33] Meanwhile, the five-ring tubular with vacancies will become more and more stable. For example, the quasi-planar B_{70} with the C_{3v} symmetry is slightly less stable than a five-ring tubular isomer with the D_{5h} symmetry, close to the average formation energy of closed shell B_{80} fullerene.

Note that the tubular structure B_{76} with D_{4h} symmetry is more stable than the B_{80} cage. Within our computational capabilities, we have calculated the six-ring and five-ring with various vacancies with $n < 80$, where the tubular structure B_{76} is found to be a magic structure with high stability. The most stable B_{70} and B_{76} tubular clusters constructed by the nanoribbon with the units of 14 and 19 atoms are shown in Figure S6, where the structural stabilities of the similar tubular clusters depend on the diameter. Table S1 in the Supporting Information lists the HOMO−LUMO (H-L) energy gaps of B_n clusters from various methods, indicating the same tendency for the B_{80} cage and the tubular clusters. The gap of the B_{80} cage is about 1.4 eV according to HSE calculations, and the hollow cylindrical cluster B_{76} is around 1.2 eV. Compared to the metallic B_{70} of quasi-planar structure, the tubular B_{70} possesses a relative high chemical stability with an H-L gap of about 1 eV. As the H-L gaps of B_{76} and B_{70} are larger than the B_{84} planar, it indicates the potential superiority of the cylindrical structures.

Carbon nanotubes, hollow cages, and planar graphene nanoflakes have similar motifs with the planar sheet of graphene, attributed to the stable sp^2 hybridizations of carbon. As shown above, stable boron nanostructures with the number of boron atoms from 30 to 84 can be planar, tubular, and cage-like, containing the triangle and polygon vacancies. For most nanostructures, the tubular structures should be more stable than the planar ones, since the edge atoms with less coordination number might destabilize the system. However, the edge in boron nanostructures is necessary for the

DOI: 10.1021/acs.jpcc.7b03359
J. Phys. Chem. C 2017, 121, 11950−11955

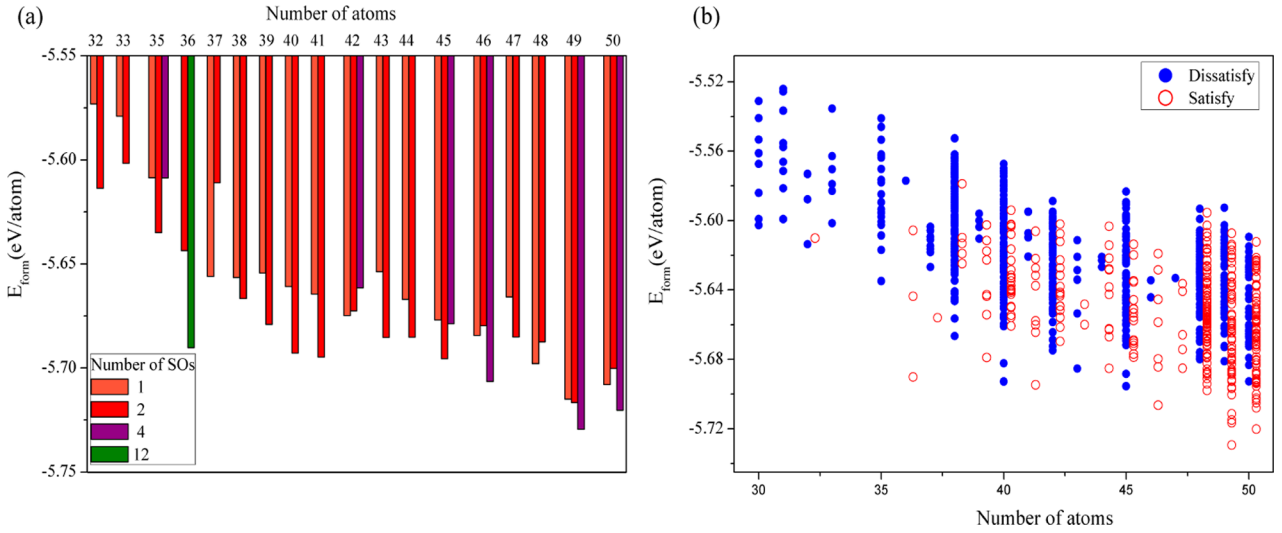

Figure 4. Relation of the E_{form} and the size of the B_n (n = 30−50) clusters. (a) The colorful bars represent the number of the symmetry operation (SOs) for the corresponding B_n clusters. (b) The results of the 8-electron model solutions for all the isomers. The empty dots represent that there exists a solution for the model; the solid dots represent that there does not exist a solution for the model.

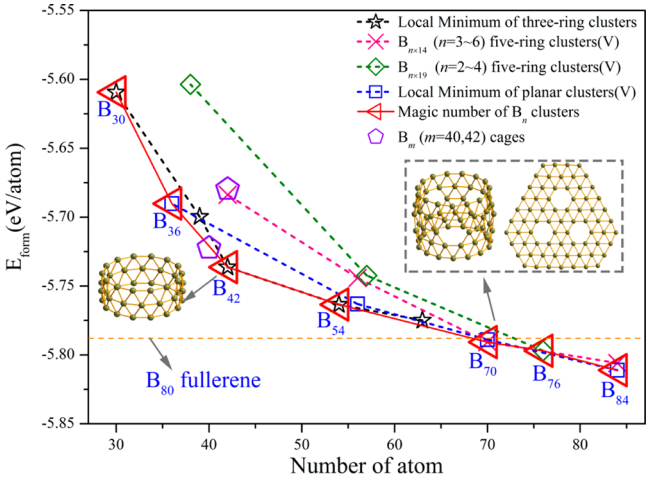

Figure 5. Relation of the E_{form} and the size of the B_n (n = 30−85) clusters. The empty stars represent the local minimum of the three-ring tubular clusters, the empty squares represent the local minimum of the quasi-planar clusters, the cross and the empty diamonds represent the five-ring tubular clusters rolled by the ribbon [unit (14, 19)], the empty triangles represent the magic number B_n clusters, and the empty pentagons represent the B_n cages.

distribution of 2c-2e bonds, according to our model and the analysis of electron localization function (ELF). The complicated bonding of B is characterized with both localized bonding and delocalized bonding, where the 8-electron rule indicates the localization and the variance of 2c-2e and 3c-2e bonds' distribution is minimized to describe the delocalized bonding. Applying the former adaptive natural density partitioning (AdNDP) method[47] to analyze the (nc-2e) bond is very difficult for the large B_n clusters, and the results might be dependent on the user's experience.

On the basis of the 2c-2e and 3c-2e bond model, we adopt the 8-electron rule to analyze the magic clusters of high stabilities. The double-ring B_{20} is a highly stable cluster with a large H-L energy gap of over 2 eV, which is regarded as the embryo of single-walled boron nanotubes.[16] As shown in Figure S7a, there is a 3c-2e bond in every triangle and the edge bonds are the 2c-2e bond with an occupation of 1/2, in agreement with the isosurface charge difference. For the stable tubular B_{42} cluster, the occupation of the 2c-2e bond on the edge is 3/4, while there are two occupations (1/2 and 1) of the 3c-2e bond for the triangles. With the decrease of the ELF isosurface value, the area with the 2c-2e bonds with the occupation of 3/4 and the 3c-2e bonds with the occupation of 1 become visible first (shown in the Figure S7b-4), followed by the 3c-2e bonds with the occupation number of 1/2.

Figure 6a shows the model analysis and ELF for the bonding in the stable quasi-planar B_{84}. Similarly, at a large isovalue of 0.86 for B_{84}, the charge distribution on the profile and the hexagonal vacancies become visible first, followed by the triangles with the 3c-2e bond with the occupation number of 1. At a smaller isovalue of 0.74, the charge distribution of a half 3c-2e bond is visible. According to our bonding analysis (shown in Figure 6a-4), there are 48 (24) 3c-2e (2c-2e) bonds with the occupation of 1, 72 (18) 3c-2e (2c-2e) bonds with the occupation of 1/2, and 12 2c-2e bonds with the occupation of 3/4, maintaining the symmetry of B_{84}. Thus, our model can give a better understanding of the bonding in boron clusters, where the 2c-2e and 3c-2e bonds are distributed to satisfy the 8-electron rule.

As shown in Figure 6b, the charge distribution along the B−B bond at the peripheral edge is visible at first, followed by the one along the hexagonal vacancies as the ELF isovalue decreased from 0.92 to 0.84. Note that the B−B bond length along the peripheral edge is 1.61 Å, which is shorter than the one (1.69 Å) along the hexagonal vacancies, indicating the strong electron localization along the peripheral edge. According to our bond model, we have a possible solution for the B_{76} cluster. As shown in Figure 6b-6, there are 32 3c-2e bonds with the occupations of 1 and 3/4, 40 2c-2e bonds with the occupation of 3/4, and 40 (16) 3c-2e (2c-2e) bonds with the occupations of 1/2. In the hexagonal vacancies, the 2c-2e bonds parallel to the peripheral edge possess a higher occupation number (3/4) than the other 2c-2c bonds (1/2), which is consistent with the first visible charge distribution. Importantly, all the stable B_n (n = 30−85) clusters (the red triangles in Figure 4) can be understood by our bond model

DOI: 10.1021/acs.jpcc.7b03359
J. Phys. Chem. C 2017, 121, 11950−11955

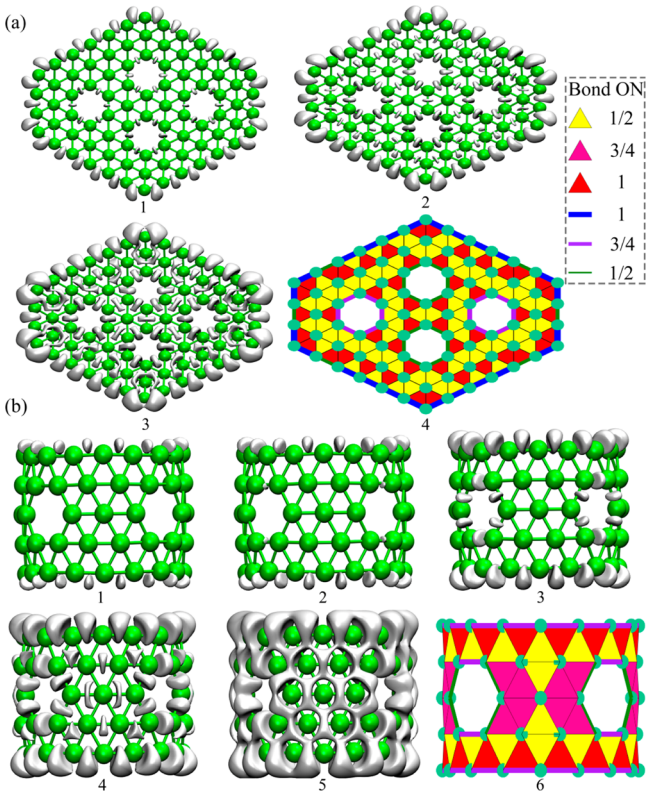

Figure 6. Electron localization function (ELF) at various values and bonding analysis for the B_{84} quasi-planar clusters (a) and the stable B_{76} tubular clusters (b). (a-1−3) represent the isovalues of 0.86, 0.81, and 0.74, respectively; (a-4) represents the distribution of 2c-2e and 3c-2e bonds. The occupation numbers of the 2c-2e and 3c-2e bonds are listed on the right side. (b-1−5) represent the isovalues of 0.92, 0.90, 0.84, 0.78 and 0.71, respectively; (b-6) represents the distribution of 2c-2e and 3c-2e bonds.

with a clear and simple picture (Figures S8−S10), indicating that our model is an effective and universal method to analyze the electron distribution in the planar, tubular, and cage-like boron nanostructures.

4. CONCLUSION

In summary, we have investigated the stability and electronic properties of the tubular and quasi-planar B_n (n = 50−85) clusters based on the first-principles calculations. We have proposed a practical criterion for screening the initial candidates, providing a better understanding of bonding in boron nanostructures consistent with the charge distribution from first-principles calculations. Interestingly, there are quasi-planar and tubular isomers of B_{70} as stable as the B_{80} cage, while the tubular B_{76} with the D_{4h} symmetry is more stable than the B_{80} cage. According to our model, the vacancy and the edge are important to stabilize the boron nanostructures, which explains why the quasi-planar and tubular boron nanostructures could be as stable as the cages. In addition, the core−shell isomers would be also stable as the number of B atoms increases, and we might extend our model with the 8-electron rule for these structures in the future. Our finding may stimulate a brand new way to design the reasonable boron clusters and to understand the novel chemical bonding in boron nanostructures.

ASSOCIATED CONTENT

Supporting Information

The Supporting Information is available free of charge on the ACS Publications website at DOI: 10.1021/acs.jpcc.7b03359.

Modeling details and the calculated results for the B_n clusters (PDF)

AUTHOR INFORMATION

Corresponding Authors

*E-mail: scxbyang@scut.edu.cn (X.-B.Y.).
*E-mail: xu.h@sustc.edu.cn (H.X.).

ORCID

Xiao-Bao Yang: 0000-0001-8851-1988
Hu Xu: 0000-0002-2254-5840

Notes

The authors declare no competing financial interest.

ACKNOWLEDGMENTS

This work was supported by the National Natural Science Foundation of China (Nos. 11474100, 11674148), Guangdong Natural Science Funds for Distinguished Young Scholars (No. 2014A030306024), and the Basic Research Program of Science, Technology and Innovation Commission of Shenzhen Municipality (Grant No. JCYJ20160531190054083).

REFERENCES

(1) Albert, B.; Hillebrecht, H. Boron: Elementary Challenge for Experimenters and Theoreticians. *Angew. Chem., Int. Ed.* **2009**, *48*, 8640−8668.
(2) Alexandrova, A. N.; Boldyrev, A. I.; Zhai, H.-J.; Wang, L.-S. All-Boron Aromatic Clusters as Potential New Inorganic Ligands and Building Blocks in Chemistry. *Coord. Chem. Rev.* **2006**, *250*, 2811−2866.
(3) Sergeeva, A. P.; Popov, I. A.; Piazza, Z. A.; Li, W. L.; Romanescu, C.; Wang, L. S.; Boldyrev, A. I. Understanding Boron through Size-Selected Clusters: Structure, Chemical Bonding, and Fluxionality. *Acc. Chem. Res.* **2014**, *47*, 1349−58.
(4) Boldyrev, A. I.; Wang, L. S. Beyond Organic Chemistry: Aromaticity in Atomic Clusters. *Phys. Chem. Chem. Phys.* **2016**, *18*, 11589−11605.
(5) Fujimori, M.; Nakata, T.; Nakayama, T.; Nishibori, E.; Kimura, K.; Takata, M.; Sakata, M. Peculiar Covalent Bonds in α-Rhombohedral Boron. *Phys. Rev. Lett.* **1999**, *82*, 4452−4455.
(6) Piazza, Z. A.; Li, W. L.; Romanescu, C.; Sergeeva, A. P.; Wang, L. S.; Boldyrev, A. I. A Photoelectron Spectroscopy and *Ab Initio* Study of B_{21}^-: Negatively Charged Boron Clusters Continue to Be Planar at 21. *J. Chem. Phys.* **2012**, *136*, 104310.
(7) Sergeeva, A. P.; Piazza, Z. A.; Romanescu, C.; Li, W. L.; Boldyrev, A. I.; Wang, L. S. B_{22}^- and B_{23}^-: All-Boron Analogues of Anthracene and Phenanthrene. *J. Am. Chem. Soc.* **2012**, *134*, 18065−73.
(8) Popov, I. A.; Piazza, Z. A.; Li, W. L.; Wang, L. S.; Boldyrev, A. I. A Combined Photoelectron Spectroscopy and *Ab Initio* Study of the Quasi-Planar B_{24}^- Cluster. *J. Chem. Phys.* **2013**, *139*, 144307.
(9) Piazza, Z. A.; Popov, I. A.; Li, W. L.; Pal, R.; Zeng, X. C.; Boldyrev, A. I.; Wang, L. S. A Photoelectron Spectroscopy and *Ab Initio* Study of the Structures and Chemical Bonding of the B_{25}^- Cluster. *J. Chem. Phys.* **2014**, *141*, 034303.
(10) Li, W. L.; Zhao, Y. F.; Hu, H. S.; Li, J.; Wang, L. S. $[B_{30}]^-$: A Quasiplanar Chiral Boron Cluster. *Angew. Chem., Int. Ed.* **2014**, *53*, 5540−5.
(11) Li, W. L.; Chen, Q.; Tian, W. J.; Bai, H.; Zhao, Y. F.; Hu, H. S.; Li, J.; Zhai, H. J.; Li, S. D.; Wang, L. S. The B_{35} Cluster with a Double-Hexagonal Vacancy: A New and More Flexible Structural Motif for Borophene. *J. Am. Chem. Soc.* **2014**, *136*, 12257−60.

(12) Piazza, Z. A.; Hu, H. S.; Li, W. L.; Zhao, Y. F.; Li, J.; Wang, L. S. Planar Hexagonal B_{36} as a Potential Basis for Extended Single-Atom Layer Boron Sheets. *Nat. Commun.* **2014**, *5*, 3113.
(13) Li, W. L.; Pal, R.; Piazza, Z. A.; Zeng, X. C.; Wang, L. S. B_{27}^-: Appearance of the Smallest Planar Boron Cluster Containing a Hexagonal Vacancy. *J. Chem. Phys.* **2015**, *142*, 204305.
(14) Oger, E.; Crawford, N. R.; Kelting, R.; Weis, P.; Kappes, M. M.; Ahlrichs, R. Boron Cluster Cations: Transition from Planar to Cylindrical Structures. *Angew. Chem., Int. Ed.* **2007**, *46*, 8503−6.
(15) Tai, T. B.; Nguyen, M. T. Electronic Structure and Photoelectron Spectra of B_n with n = 26−29: An Overview of Structural Characteristics and Growth Mechanism of Boron Clusters. *Phys. Chem. Chem. Phys.* **2015**, *17*, 13672−9.
(16) Kiran, B.; Bulusu, S.; Zhai, H. J.; Yoo, S.; Zeng, X. C.; Wang, L. S. Planar-to-Tubular Structural Transition in Boron Clusters: B_{20} as the Embryo of Single-Walled Boron Nanotubes. *Proc. Natl. Acad. Sci. U. S. A.* **2005**, *102*, 961−4.
(17) Zhao, J.; Huang, X.; Shi, R.; Liu, H.; Su, Y.; King, R. B. B_{28}: The Smallest All-Boron Cage from an Ab Initio Global Search. *Nanoscale* **2015**, *7*, 15086−15090.
(18) Wang, Y.-J.; et al. Observation and Characterization of the Smallest Borospherene, B_{28}^- and B_{28}. *J. Chem. Phys.* **2016**, *144*, 064307.
(19) Li, H.-R.; et al. Competition between Quasi-Planar and Cage-Like Structures in the B_{29}^- Cluster: Photoelectron Spectroscopy and *Ab Initio* Calculations. *Phys. Chem. Chem. Phys.* **2016**, *18*, 29147−29155.
(20) Lv, J.; Wang, Y.; Zhu, L.; Ma, Y. B_{38}: An All-Boron Fullerene Analogue. *Nanoscale* **2014**, *6*, 11692−11696.
(21) Chen, Q.; et al. Experimental and Theoretical Evidence of an Axially Chiral Borospherene. *ACS Nano* **2015**, *9*, 754−760.
(22) Zhai, H. J.; et al. Observation of an All-Boron Fullerene. *Nat. Chem.* **2014**, *6*, 727−731.
(23) Liu, H.; Gao, J.; Zhao, J. From Boron Cluster to Two-Dimensional Boron Sheet on Cu(111) Surface: Growth Mechanism and Hole Formation. *Sci. Rep.* **2013**, *3*, 3238.
(24) Xu, S. G.; Zhao, Y. J.; Liao, J. H.; Yang, X. B.; Xu, H. The Nucleation and Growth of Borophene on the Ag (111) Surface. *Nano Res.* **2016**, *9*, 2616−2622.
(25) Liu, Y.; Penev, E. S.; Yakobson, B. I. Probing the Synthesis of Two-Dimensional Boron by First-Principles Computations. *Angew. Chem., Int. Ed.* **2013**, *52*, 3156−3159.
(26) Zhang, Z.; Yang, Y.; Gao, G.; Yakobson, B. I. Two-Dimensional Boron Monolayers Mediated by Metal Substrates. *Angew. Chem., Int. Ed.* **2015**, *54*, 13022−13026.
(27) Mannix, A. J.; et al. Synthesis of Borophenes: Anisotropic, Two-Dimensional Boron Polymorphs. *Science* **2015**, *350*, 1513−1516.
(28) Feng, B. J.; Zhang, J.; Zhong, Q.; Li, W. B.; Li, S.; Li, H.; Cheng, P.; Meng, S.; Chen, L.; Wu, K. H. Experimental Realization of Two-Dimensional Boron Sheets. *Nat. Chem.* **2016**, *8*, 563−568.
(29) Castro Neto, A. H.; Guinea, F.; Peres, N. M. R.; Novoselov, K. S.; Geim, A. K. The Electronic Properties of Graphene. *Rev. Mod. Phys.* **2009**, *81*, 109−162.
(30) Gonzalez Szwacki, N.; Sadrzadeh, A.; Yakobson, B. I. B_{80} Fullerene: An *Ab Initio* Prediction of Geometry, Stability, and Electronic Structure. *Phys. Rev. Lett.* **2007**, *98*, 166804.
(31) Tang, H.; Ismail-Beigi, S. Novel Precursors for Boron Nanotubes: The Competition of Two-Center and Three-Center Bonding in Boron Sheets. *Phys. Rev. Lett.* **2007**, *99*, 115501.
(32) Yang, X.; Ding, Y.; Ni, J. *Ab Initio* Prediction of Stable Boron Sheets and Boron Nanotubes: Structure, Stability, and Electronic Properties. *Phys. Rev. B: Condens. Matter Mater. Phys.* **2008**, *77*, 041402.
(33) Rahane, A. B.; Kumar, V. B_{84}: A Quasi-Planar Boron Cluster Stabilized with Hexagonal Holes. *Nanoscale* **2015**, *7*, 4055−4062.
(34) Xu, S.-G.; Zhao, Y.-J.; Liao, J.-H.; Yang, X.-B. Understanding the Stable Boron Clusters: A Bond Model and First-Principles Calculations Based on High-Throughput Screening. *J. Chem. Phys.* **2015**, *142*, 214307.
(35) Curtarolo, S.; Hart, G. L. W.; Nardelli, M. B.; Mingo, N.; Sanvito, S.; Levy, O. The High-Throughput Highway to Computational Materials Design. *Nat. Mater.* **2013**, *12*, 191−201.
(36) Kresse, G.; Furthmüller, J. Efficient Iterative Schemes for *Ab Initio* Total-Energy Calculations Using a Plane-Wave Basis Set. *Phys. Rev. B: Condens. Matter Mater. Phys.* **1996**, *54*, 11169−11186.
(37) Kresse, G.; Joubert, D. From Ultrasoft Pseudopotentials to the Projector Augmented-Wave Method. *Phys. Rev. B: Condens. Matter Mater. Phys.* **1999**, *59*, 1758−1775.
(38) Perdew, J. P.; Burke, K.; Ernzerhof, M. Generalized Gradient Approximation Made Simple. *Phys. Rev. Lett.* **1996**, *77*, 3865−3868.
(39) Perdew, J. P.; Burke, K.; Ernzerhof, M. Generalized Gradient Approximation Made Simple (Vol 77, Pg 3865, 1996). *Phys. Rev. Lett.* **1997**, *78*, 1396−1396.
(40) Delley, B. An All - Electron Numerical Method for Solving the Local Density Functional for Polyatomic Molecules. *J. Chem. Phys.* **1990**, *92*, 508−517.
(41) Delley, B. From Molecules to Solids with the $Dmol^3$ Approach. *J. Chem. Phys.* **2000**, *113*, 7756−7764.
(42) Heyd, J.; Scuseria, G. E.; Ernzerhof, M. Hybrid Functionals Based on a Screened Coulomb Potential. *J. Chem. Phys.* **2003**, *118*, 8207−8215.
(43) Paier, J.; Marsman, M.; Hummer, K.; Kresse, G.; Gerber, I. C.; Ángyán, J. G. Erratum: "Screened Hybrid Density Functionals Applied to Solids" [J. Chem. Phys. 124, 154709 (2006)]. *J. Chem. Phys.* **2006**, *125*, 249901.
(44) Tian, F.-Y.; Wang, Y.-X. The Competition of Double-, Four-, and Three-Ring Tubular B_{3n}(n = 8−32) Nanoclusters. *J. Chem. Phys.* **2008**, *129*, 024903.
(45) Özdoğan, C.; Mukhopadhyay, S.; Hayami, W.; Güvenç, Z. B.; Pandey, R.; Boustani, I. The Unusually Stable B_{100} Fullerene, Structural Transitions in Boron Nanostructures, and a Comparative Study of α- and γ-Boron and Sheets. *J. Phys. Chem. C* **2010**, *114*, 4362−4375.
(46) Chen, Q.; et al. Cage-Like B_{41}^+ and B_{42}^{2+}: New Chiral Members of the Borospherene Family. *Angew. Chem., Int. Ed.* **2015**, *54*, 8160−8164.
(47) Zubarev, D. Y.; Boldyrev, A. I. "Developing Paradigms of Chemical Bonding: Adaptive Natural Density Partitioning. *Phys. Chem. Chem. Phys.* **2008**, *10*, 5207−5217.

DOI: 10.1021/acs.jpcc.7b03359
J. Phys. Chem. C 2017, 121, 11950−11955